HHS Public Access

Author manuscript

Environ Sci Technol. Author manuscript; available in PMC 2018 November 28.

Published in final edited form as:

Environ Sci Technol. 2013 February 19; 47(4): 1844–1852. doi:10.1021/es3030337.

Chirality Affects Aggregation Kinetics of Single-Walled Carbon Nanotubes

Iftheker A. Khan[†], **A. R. M. Nabiul Afrooz**[†], **Joseph R. V. Flora**[†], **P. Ariette Schierz**[‡], **P. Lee Ferguson**[§], **Tara Sabo-Attwood**[‖], and **Navid B. Saleh**[*,†]

[†]Department of Civil and Environmental Engineering, University of South Carolina, Columbia, South Carolina 29208, United States

[‡]Department of Civil, Architectural, and Environmental Engineering, University of Texas, Austin, Texas 78712, United States

[§]Department of Civil and Environmental Engineering, Duke University, Durham, North Carolina 27708, United States

[‖]Department of Environmental and Global Health, University of Florida, Gainesville, Florida 32610, United States

Abstract

Aggregation kinetics of chiral-specific semiconducting single-walled carbon nanotubes (SWNTs) was systematically studied through time-resolved dynamic light scattering. Varied monovalent (NaCl) and divalent ($CaCl_2$) electrolyte composition was used as background solution chemistry. Suwannee River humic acid (SRHA) was used to study the effects of natural organic matter on chirally separated SWNT aggregation. Increasing salt concentration and introduction of divalent cations caused aggregation of SWNT clusters by suppressing the electrostatic repulsive interaction from the oxidized surfaces. The (6,5) SWNTs, i.e., SG65, with relatively lower diameter tubes compared to (7,6), i.e., SG76, showed substantially higher stability (7- and 5-fold for NaCl and $CaCl_2$, respectively). The critical coagulation concentration (CCC) values were 96 and 13 mM NaCl in the case of NaCl and 2.8 and 0.6 mM $CaCl_2$ for SG65 and SG76, respectively. The increased tube diameter for (7,6) armchair SWNTs likely presented with higher van der Waals interaction and thus increased the aggregation propensity substantially. The presence of SRHA enhanced SWNT stability in divalent $CaCl_2$ environment through steric interaction from adsorbed humic molecules; however showed little or no effects for monovalent NaCl. The mechanism of aggregation—describing favorable interaction tendencies for (7,6) SWNTs—is probed through ab initio molecular modeling. The results suggest that SWNT stability can be chirality dependent in typical aquatic environment.

[*]**Corresponding Author:** salehn@engr.sc.edu; phone: (803) 777-2288.

ASSOCIATED CONTENT

Supporting Information

Additional text, table, and figures as noted in the manuscript. This information is available free of charge via the Internet at http://pubs.acs.org/.

Notes

The authors declare no competing financial interest.

Graphical Abstract

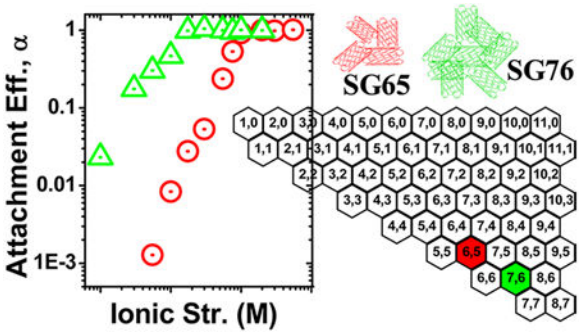

INTRODUCTION

Tessellated hexagonal rings of carbon, when coiled to form unidimensionally curved tubular structures named single-walled carbon nanotubes (SWNTs), provide superior mechanical, electrical, and optical properties.[1] Variation in helicity and diameter of these SWNTs, represented as chirality, can induce significant changes in their electrokinetic surface properties.[2] Change in SWNT chirality results in electron confinement differences, which causes electron transport variation along the SWNT axes and thus exhibits unique physicochemical, electronic, and optical properties.[3–5] These hallmark characteristics of SWNTs have versatile applicability in various fields that include, but are not limited to, energy storage and energy conversion, molecular electronics, nanocomposite, nanoprobes and sensors, and construction industries.[4] In addition, biochemical sensors acquired better sensing selectivity using chiral-specific SWNTs.[5] Many such applications, e.g., molecular electronic devices in high-speed computers, biochemical sensors in diagnostics, composite materials, etc., have high likelihood to be released in natural environment, either during use or at the end of life of these products and devices. The large market share, 1000 tons per year global production volume,[6] and potential environmental release of SWNTs necessitate careful evaluation of their environmental safety.

Atomic structure of SWNTs primarily depends on the amount of “twist” that the honeycomb carbon lattices undergo during nanotube formation. Such atomic orientation of the carbon atoms is reflected through chiral indices, i.e., radius (r) and chiral angle (θ).[2] In addition to surface electron properties, chirality can also govern the amount of electrochemically available surface area[2,7] and other properties.[8] Chiral vector $\left(\vec{C} = n\vec{a}_1 + m\vec{a}_2\right)$ of SWNTs thus dictates the position of “Fermi level” for carbon nanotubes and thereby their electrical conductivity.[4] Depending on the magnitudes of chiral vector components (n,m), SWNTs can either be metallic—when ($n-m$) is divisible by 3—or otherwise semiconductive.

Chirality of SWNTs also plays a dominant role in deciding the available surface area for physicochemical reaction and amount of interaction energy between tubes.[8] Such chiral dependence of interparticular energy most likely originates from change in the van der Waals interaction intensity among SWNTs;[9] which in turn regulates the overall Derjaguin, Landau, Verwey, and Overbeek (DLVO) forces of these materials.[10] Theoretical studies

show evidence of chiral dependence of DLVO forces for SWNTs; e.g., armchair tubes show stronger intermolecular forces compared to chiral or zigzag nanotubes.[11] Moreover, some studies show that such forces differ among chiral, metallic, and semiconductive SWNTs.[12] Such chirality-dependent DLVO interaction clearly indicates the potential role of helicity in controlling SWNT aggregation behavior.

Aggregation is one of the key factors that govern fate and transport of nanomaterials in natural environment.[13] Once released, carbon nanotubes (CNTs) have a strong propensity to aggregate in aqueous systems due to their high hydro-phobicity and intense attraction between tubes, evolved from the pronounced "sp^3 nature" of their structural configuration.[13] To-date, CNT aggregation literature focuses on systematic studies of SWNTs and multiwalled carbon nanotubes (MWNTs), elucidating role of physical attributes (e.g., size and shape),[14] surrounding solution chemistry (i.e., pH, ionic composition, ionic strength, presence of macromolecules, and natural organic matter),[14–17] functionalization,[18,19] and pre-treatment.[20,21] However, chiral literature for SWNTs has mostly focused on chiral separation and characterization[22,23] to extract unique structural, spectroscopic, energetic, optical, mechanical, and vibrational properties[23,24] and organic sorption characteristics.[25] There is a paucity of systematic studies focusing on the role of chirality on SWNT aggregation and thus generates a crucial data gap in SWNT fate and transport literature.

The objective of this paper is to systematically study the aggregation behavior of chiral specific SWNTs in environmentally relevant chemistries. SWNTs with (6,5), and (7,6) chiral enrichments are carefully functionalized to obtain uniform SWNT suspensions of comparable surface functionality. Detailed physicochemical and electrokinetic characterizations are performed using near-infrared (NIR) spectroscopy, X-ray photoelectron spectroscopy (XPS), Raman spectroscopy, transmission electron microscopy (TEM), and electrophoretic mobility (EPM) measurements. Fundamental aggregation kinetics of the functionalized SWNTs is performed using time-resolved dynamic light scattering (TRDLS) in the presence of a wide range of mono- and divalent electrolytes and Suwannee River humic acid (SRHA). Aggregation mechanism is elucidated using measured physicochemical properties and chirality specific ab initio interaction energy calculations.

MATERIAL AND METHODS

Chiral SWNTs.

CoMoCat SWNTs were procured from SouthWest NanoTechnologies Inc. (SWeNT, Norman, OK, USA). Two different types of SWNTs were tested in this study: SG65 (lot 000–0031) and SG76 (lot 0020).

Optimized Covalent Functionalization of SWNTs.

The SWNTs were covalently functionalized following a two-step process. Five mg of relatively pure SWNTs (with >97.5% purity) was bath sonicated for 1 h (Branson 1510) in 2.5 mL of 6 M HNO_3 to remove most metal impurities.[26] Later, the purified SWNTs were bath sonicated with 2.5 mL of concentrated H_2SO_4/HNO_3 mixture (3:1, 98% and 70% strength, respectively) for 4 h.[26,27] After each step, the SWNT suspension was filtered

through 200-nm polypropylene (GHP) membranes (Pall Life Science, Port Washington, NY) and rinsed with Milli-Q water until the pH of the filtrate reached ~6.5. The filtered sample was then dried for 3 h at 60 °C and kept in a silica gel chamber for 3 days. The conditions, i.e., sonication intensity, duration, oxidant composition, etc., were optimized using previously established sonication techniques[28] to achieve near-equal surface functionalization as verified by parallel characterization with XPS, Raman spectroscopy, and EPM measurements.

Characterization of SWNTs.

SWNT samples were characterized to determine the chirality and key physicochemical properties by employing NIR spectroscopy, TEM, XPS, Raman spectroscopy, and EPM measurements.

For NIR spectroscopy, SWNT suspensions were prepared in 2% w/w sodium deoxycholate, SDC (Sigma Aldrich) in deionized water (1 mg of SWNT per mL of SDC). The mixtures were then ultrasonicated for 10 min with a microtip ultrasonic dismembrator (Sonifier 450, Branson Ultrasonics, Danbury, CT) in a saltwater ice bath and subsequently centrifuged for 10 min under 17 860*g*. The supernatant was removed and diluted for spectroscopic characterization.[29] The pH of all samples was in the range of 6.0−7.0. NIR absorbance and fluorescence spectra of suspended individual SWNT were measured using the Nanospectralyzer NS1 (Applied Nano-fluorescence, Houston, TX) with 3 discrete laser excitation wavelengths (638, 691, and 782 nm). The integration time was 100 s with 100 spectral averages.

XPS to quantify extent of oxidation was carried out on a Kratos Axis Ultra spectrometer (Kratos Analytical Ltd., Tokyo, Japan) equipped with a hemispherical energy analyzer and monochromatic Al Kα source.[30] This source was operated at 15 keV and 150 W (10 mA) with a takeoff angle of 90° from the samples[31] and the analyses were carried out with a base pressure of 1.2×10^{-8} Torr.[32] For each sample, the XPS spectra were collected at least three times at independent spatial locations. XPS data fitting was performed using CasaXPS software.

Raman spectra—for evaluating SWNT structural signature and state of defect—were recorded using dry SWNT samples with a LabRam confocal Raman spectrophotometer (JY Horiba, HORIBA Instruments Inc., CA), equipped with a liquid nitrogen-cooled CCD detector and an He/Ne (632.817 nm) laser for excitation. Each spectrum presented is the average of at least 5 scans with integration times of 120 s for each. The relative defect state was quantified using ratio of peak areas at defect “D” band (at 1300 cm^{-1}) and characteristic “G” band (at 1600 cm^{-1}).

Morphological changes, packing structure, and purity of SWNTs upon functionalization were evaluated using TEM imaging and compared with the as-received samples. Details of TEM method are described elsewhere.[16,17] In short, 5 mL of ~15 mg/L SWNT solution was prepared in ethyl alcohol (JT Baker, ACS grade) and sonicated for 10 min using a sonic dismembrator (S-4000, Misonix). Suspensions were then placed in a bath sonicator for 15 min prior to imaging and a drop of each suspension was placed on a 200-mesh copper TEM

grid coated with carbon Formvar (Ted Pella Inc.). Excess solvent was removed by wicking with filter paper and the grid was allowed to dry in a hot plate at 75 °C for 15 min. Images were collected using an H-9500 (300 kV) TEM (Hitachi High Technologies America, Inc., CA) with 0.18-nm resolution.

The EPM values of functionalized SWNTs were measured for a range of mono- and divalent cations with a Malvern Zetasizer (ZEN 3660) system at 25 °C using established protocol described elsewhere.[16,17] In short, diluted stock solution at ~1 mg/L concentration was maintained. Electrolyte solutions at respective dilutions were added immediately prior to the EPM measurements to mimic the aggregation experiments. All EPM measurements were conducted with at least three replicate samples to ensure reproducibility.

Solution Chemistry.

SWNT aggregation was initiated by adding mono- and divalent electrolytes under environmentally relevant conditions: i.e., 1−550 mM NaCl for SG65 and 1−200 mM NaCl for SG76, while $CaCl_2$ concentration was 0.1−30 mM for both cases. The role of natural organic matter (NOM) was evaluated using 2.5 mg of TOC/L standard II Suwannee River humic acid, SRHA (International Humic Substances Society, Denver, CO) under 10 mM ionic strength (i.e., 10 mM NaCl and 7 mM NaCl with 1 mM $CaCl_2$) conditions.

Aggregation Kinetics.

The aggregation kinetics of functionalized SWNTs was studied employing a ALV/CGS-3 precision goniometer system (ALV-GmbH, Langen, Germany), equipped with a 22 mW He −Ne laser (632.8 nm wavelength) and ALV/LSE-5004 light scattering digital correlator (ALVGmbH, Langen, Germany). Operation details are similar to earlier work[16,17,33] and are presented in the Supporting Information (Section S1).

Analysis of the data was performed using rate calculation of SWNT cluster growth at the initial aggregation stages. The rate of aggregation is known to be proportional to the rate of change of R_0 with time and can be expressed as eq 1 as follows:[17]

$$k \propto \frac{1}{N}\left[\frac{\mathrm{d}R_0(t)}{\mathrm{d}t}\right]\left\{t \to 0\right\} \quad (1)$$

where k is the initial aggregation rate, and N is the SWNT particle concentration.

To eliminate influence of particle concentration that can vary between samples, a normalized unit less quantity, known as attachment efficiency or "α", is determined from the ratio of initial aggregation rate at each electrolyte condition with that of the favorable aggregation condition. Attachment efficiency α is represented using eq 2 as follows:[17]

$$\alpha = \frac{\left[\frac{dR_0(t)}{dt}\right]_{\{t \to 0\}}}{\left[\frac{dR_0(t)}{dt}\right]_{\{t \to \infty\}}} \quad (2)$$

where α is the attachment efficiency, and t is the time of aggregation. All DLS measurements were conducted at 20 ±0.5 °C and at least duplicate samples were tested to obtain significant reproducibility.

Ab Initio Calculations.

Interaction energy between SWNTs was estimated with ab initio molecular dynamics.[34] Details are presented in the SI (Section S2). Density functional theory (DFT) principles were applied through DFT-D3/BLYP/6–31G,[35,36] and interaction energy between the SWNTs was calculated using eq 3.

$$\text{Interaction energy} = E(\text{SWNT pair}) - 2E(\text{single SWNT}) \quad (3)$$

A final energy calculation was performed using the coordinates of the SWNT pair at the minimum of the interaction energy diagram. The basis set used for the carbon molecules in half of the middle third section facing each SWNT was 6–31+G(d), with a 6–31G basis set used for the remaining carbon and hydrogen atoms (Figure S2).

RESULTS AND DISCUSSION

Chiral SWNTs.

Figure 1 presents chirality charts depicting distribution of SWNT chiral structures based on the roll-up vectors. Such plots are developed using fluorescence absorbance spectra detected by NIR spectroscopy (Figure S3). It is well-known in the literature that the diameter of SWNTs generates well-defined van Hove maxima for electronic density of states that in turn causes sharp interband transitions in the absorbance spectra.[37,38] Figure S3 presents NIR spectra for SG65 and SG76 that are deconvoluted to basis function, which resulted in predictive simulated spectrum and thus the chiral distribution of the samples. The chirality charts thus obtained present relative enrichments of specific SWNT chirality through partial filling of the hexagons; i.e., the more filled a hexagon is the higher is the enrichment of that specific SWNT chirality in the analyzed sample.[39] Figure 1 demonstrates major presence of semiconducting tubes with major enrichments of (6,5) and (7,6) chiralities in the two respective samples. Overall, the chirally enrichments for the two samples are dominated by similar roll-up angle (~27°) with variable diameter (0.756 and 0.895 nm for SG65 and SG76, respectively) tubes, near armchair configuration (Figure S4). In addition, other chiralities present in minor quantities in SG65 are with near-armchair configuration (Figure 1a); i.e., (7,3), (7,5), and (8,4). The minor chiralities in SG76 on the other hand, show a wide coverage of the chirality map that span across armchair to zigzag configurations (Figure 1b);

i.e., (7,5), (9,4), (10,3), and (12,1). The values for chiral angles and diameters for all chiralities (major and minor) present in SG65 and SG76 are presented in Table S1.

Optimized Covalent Functionalization of SWNTs.

Covalent functionalization of the SWNT samples was optimized to achieve near-equal amount of oxidation. The validation of such optimization is achieved by performing multiple surface characterization measurements; i.e., XPS, Raman spectroscopy, and TEM. The XPS spectra show C1s peaks in the range of 282.2−286.0 eV binding energy (Figures S5 and S6); which confirms C−C bond signature, characteristic to graphitic structures.[40] The O1s peaks on the other hand appeared at 529.2−533.0 eV (Figures S3 and S4), indicating strong presence of carboxyl (O═C−O−) groups on the SWNTs.[40] The percentage oxidation is quantified to be 4.56 ±0.53 and 4.80 ± 0.33 for pristine and 11.90 ± 2.50 and 13.36 ±0.55 for functionalized SG65 and SG76, respectively (Figure 2a). The extent of oxidation to the SWNTs compares well with the literature reported values that varied from 1.6% to 11.3%.[41] Incorporation of surface oxygen groups through covalent acid etching process is also reported for other graphitic materials, e.g., MWNTs; which show variations from 1% to 6%, [42] 4.5% to 10.2%,[43] etc., that are in a range of oxidation similar to those reported in this article.

Parallelly, Raman spectroscopic measurements show relative presence of defects on SWNT surfaces as observed from the peak response[17] in defect or “D-band” (near 1310 to 1330 cm $^{-1}$) region with respect to the response from characteristic graphitic or “G-band” (near 1590 cm^{-1}) region (Figure S7). The ratios of areas under the peaks at D and G regions provide quantifiable relative-defect values for SG65 and SG76 chiralities. Figure 2b shows D/G ratio of 0.21 ± 0.01 and0.12 ± 0.01 for pristine that increased to 0.24 ± 0.03 and 0.25 ± 0.08 for functionalized SG65 and SG76, respectively. The literature reports a similar increase in D/G ratio for SWNTs due to mechano-chemical functionalization.[17] Such increase in the D/G ratio upon functionalization indicates C−C bond rupture and subsequent formation of C−O and O−C=O functional groups due to the presence of strong oxidants.[17,44] The combinatorial evidence of XPS and Raman spectroscopy confirms optimized oxidation through the incorporation of near-equal extent of carboxyl (COO−) surface functional groups.

Furthermore, the morphological changes upon functionalization are observed through TEM imaging. TEM micrographs of pristine and functionalized SWNTs are presented in Figure 3. Representative TEM micrographs show highly bundled and long tubular structures for both the pristine SG65 (Figure 3a) and SG76 (Figure 3b) samples. Covalent functionalization and incorporation of surface functional groups—as evident from XPS and Raman spectroscopy —caused substantial debundling of the tubes for both SG65 (Figure 3c) and SG76 (Figure 3d). In addition, shortening of tubes with sharp ends is also evident from the micrographs. The catalyst particles are also appeared to be removed through this oxidation process as evidenced from the relative absence of dense spherical features in the images (Figure 3c–d), which appear to be present in the pristine cases (Figure 3a–b). Such changes in SWNT morphology are consistently observed elsewhere in the literature.[17,45]

Electrokinetic Properties.

Electrokinetic properties of oxidized SWNTs with mono- and divalent electrolytes are presented in Figure 4. The EPM show presence of negative surface potential in SWNTs for the entire range of electrolytes. Though the origins of surface charge on all-carbon graphitic materials are unclear, previous literature evidence confirms such electrokinetic behavior for SWNTs upon oxidation or surface functionalization.[17,20] The EPM values showed gradual decrease with the increase in electrolyte concentration for both SWNT samples. For SG65 and SG76, the EPM values varied from $-(1.94 \pm 0.14) \times 10^{-8}$ to $-(0.73 \pm 0.04) \times 10^{-8}$ and from $-(1.51 \pm 0.02) \times 10^{-8}$ to $-(0.72 \pm 0.02) \times 10^{-8}$ $m^2\ V^{-1}\ S^{-1}$, respectively, for the lower and higher end of monovalent electrolyte conditions. For the change in divalent electrolyte concentration from 0.1 to 10 mM $CaCl_2$, the EPM values decreased from $-(2.05 \pm 0.33) \times 10^{-8}$ to $-(0.72 \pm 0.11) \times 10^{-8}$ and from $-(1.58 \pm 0.07) \times 10^{-8}$ to $-(0.47 \pm 0.06)$ 10^{-8} $m^2\ V^{-1}\ S^{-1}$ for SG65 and SG76, respectively. Overall, the EPM values are found to be similar between SG65 and SG76 tubes for both electrolyte types and in nearly all conditions; however, with slightly more negative EPM values for SG65 compared to that of SG76. The data reconfirm the nearly equal optimized oxidation of both the samples with an indication of slightly higher contribution toward electrostatic repulsion for the SG65 tubes. The ranges of EPM for SWNTs are consistent with previously reported findings. Both the acid treated and sonicated SWNTs show similar range of EPM, i.e., -1.24×10^{-8},[17] -0.93×10^{-8},[20] and -0.8×10^{-8} $m^2\ V^{-1}\ S^{-1}$ [46] in low electrolyte conditions. The EPM values are relatively low and show similar range with reference to SG76 values. Whereas MWNTs and fullerenes show relatively higher EPM values for both acid etching and sonication treatment cases; i.e., -2.25×10^{-8},[16] -2.2×10^{-8} (pH 6) and -3.2×10^{-8} $m^2\ V^{-1}\ S^{-1}$ (high pH)[47] for MWNTs and -3.3×10^{-8} [48] and -1.3×10^{-8} $m^2\ V^{-1}\ S^{-1}$ [49] for fullerenes.

Aggregation Kinetics.

Stability plots for SG65 and SG76 in response to a wide range of mono- and divalent electrolytes are presented in Figure 5. The attachment efficiencies presented are calculated using initial rates of aggregation for each electrolyte condition as obtained from time dependent aggregation profiles (Figure S8). The initial hydrodynamic radii of the stable SWNT clusters are found to be 117 ± 8 and 208 ± 11 nm in case of monovalent electrolyte conditions for SG65 and SG76, respectively (Figure S8a−b). For the divalent electrolyte, the initial hydrodynamic radii showed a slight increase to 126 ± 15 and 226 ± 14 nm for SG65 and SG76, respectively (Figure S8c−d). The key feature of the stability plots is the well-defined aggregation regimes, i.e., reaction limited (RLCA) or unfavorable and diffusion limited (DLCA) or favorable aggregation regimes; which demonstrate a typical DLVO type interaction between tubes. With the increase in NaCl concentration (Figure 5a), the SG65 shows a substantially higher stability compared to SG76. Also, the SG65 tubes' response to the first logarithmic increase of NaCl is relatively weak compared to the remainder of the RLCA regime—unlike the SG76 behavior—which also demonstrates higher stability to electrolyte concentration increase. The critical coagulation concentration (CCC) values estimated from the RLCA and DLCA regime slopes are 96 and 13 mM NaCl for SG65 and SG76, respectively. The CCC values provide further evidence of higher stability— >7 fold higher CCC—for SG65 compared to SG76.

Similarly, the stability plots for divalent $CaCl_2$ present similar key features that include defined RLCA and DLCA, higher stability of SG65 compared to SG76, and weak response for the first logarithmic increase of electrolyte concentration for SG65. The CCC values estimated were 2.8 and 0.6 mM $CaCl_2$ for SG65 and SG76, respectively— >5 fold increase in CCC for SG65 compared to that of SG76. The CCC values between mono- and divalent cations follow z^n dependence as per Schultz−Hardy Rule (n = 2 to 6), with n = 5.10 and 4.44 for SG65 and SG76, respectively.[13]

The literature findings for aggregation of SWNTs are in a similar range with respect to CCC values obtained in this study, with the exception of SG65 monovalent aggregation case. Nitric acid treated SWNTs in literature showed relatively low values of CCC, i.e., 37 mM NaCl and 0.2 mM $CaCl_2$,[20] compared to SG65 in this study. The literature value for acid etched SWNTs are comparable to mechanically functionalized SWNT CCC with reported values of 20 mM NaCl and 2.0 mM $CaCl_2$.[17] Such reported values are thus similar to SG76 aggregation results. However, the chirality and diameter distribution of these SWNTs[16,20] are unknown and thus may not bear mechanistic significance to the results obtained in this study. On the other hand, literature reported relatively high colloidal stability for acid functionalized MWNTs with CCC values of 93 mM of NaCl and 1.2 mM of $CaCl_2$;[47] while the sonication treatment resulted in lower SWNT stability with CCC of 25 mM NaCl and 2.6 mM $CaCl_2$.[16] It is to be noted that CCC values for fullerenes are consistently reported to be high with 85−160 mM NaCl and 4.1−6.0 mM $CaCl_2$.[48,49]

Aggregation Mechanism and the Role of Chirality.

Aggregation of colloids is dominated by the relative interplay between inherent van der Waals attractive and electrostatic repulsive interactions. The SWNTs are known to have high aggregation propensity due to their strong van der Waals interaction.[50,51] In this study, the electrostatic interactions for both tubes were similar, however they showed a maximum difference in EPM of $0.43 \pm 0.14 \times 10^{-8}$ m^2 V^{-1} S^{-1} between SG65 and SG76 SWNTs. Such difference will likely cause higher electrostatic stabilization of SG65 compared to SG76. Earlier literature presented aggregation behavior of MWNTs, systematically studied for a wide range of oxidation states.[18,52] Even a ~1.0×10^{-8} and 0.45×10^{-8} m^2 V^{-1} S^{1-} EPM difference in these studies showed only ~4-fold and ~2.3-fold difference in the CCC values.[18,52] Thus the large difference in CCC values observed in this study is not likely due to the effects of electrokinetics only. The differences in van der Waals interaction between SG65 and SG76 samples have likely played a dominant role in the aggregation of these SWNTs. It is to be noted that SG65 has (6,5) chiral enrichment where the minor chiralities are near the armchair configuration (Table S1). In comparison, SG76 tubes have (7,6) chiral enrichment with the minor chiralities covering a wide region of the chirality chart (Table S1 and Figure S4). The notable features for SG65 is the (6,5) chiral enrichment are high roll-up angle of 27° (similar to that of (7,6), which is 27.5°) and the smallest diameter (0.76 nm) among all chiralities present. The roll-up angles for the minor chiralities are also high (17.1° −24.5°) and their diameters remain relatively small (0.70−0.84 nm) for SG65 sample. On the other hand, the SG76 with (7,6) chiral enrichment has a relatively larger diameter (0.893 nm) compared to that of (6,5). Furthermore, the minor chiralities for SG76 show relatively wider range of roll-up angle variation(3.6°−27°) and larger diameters (0.83−0.99 nm).

Literature findings show that increase in SWNT diameter increases the Hamaker constant value and thus enhances the van der Waals interaction, substantially.[53] The theoretical prediction of Hamaker constant using Lifshitz formulation with a model [14,14,m] water medium shows diameter dependence for Hamaker constant of SWNTs with armchair configurations.[53] It also shows that Hamaker constant values can be even negative for lower diameters (below 0.98 nm for this theoretical case), i.e., adding to the repulsive stabilizing interaction component in the DLVO formulation. However, the values showed to consistently increase with the increase in SWNT diameter (beyond 0.98 nm value).[53] Based on this evidence it can be concluded that SG65 with smaller diameter tubes had lower—even negative—contribution from van der Waals interaction, while SG76 with larger diameter tubes acquired a substantially higher van der Waals contribution to destabilize the SWNTs. The key mechanism responsible for lower stability of SG76 compared to SG65 is therefore the increased van der Waals attractive interaction that overshadowed the electrokinetic repulsive contribution from the covalent functionalization.

To further evaluate the aggregation mechanism, ab initio calculations are performed to calculate the interaction energies between SG65 and SG76 molecule pairs. The optimized lengths of a repeating unit of SG65 and SG76 are computed as4.17 and 4.91 nm, while optimized diameters are found to be0.76 and 0.90 nm, respectively. Such values correspond well with those reported in Table S1. The rigid molecule potential energy surface scan shows more favorable maximum interaction energy of −34.2 and −132.8 kcal/mol for SG76 compared to −30.7 and −103.8 kcal/mol for SG65 in cases of perpendicular and parallel configurations, respectively (Figure 6). A larger diameter results in less curvature and more interaction between SG76 because of the higher overlap between π electrons. Similar simulation results were reported by Aich et al.,[33] where the interaction energy between fullerene pairs becomes more favorable as the fullerene radii increases from C60 to C84. The final interaction energies calculated with a higher level basis set for the lowest point in Figure 6 report −29.1 and −33.0 kcal/mol for SG65 and SG76, respectively; confirming that the difference in the interaction energy between SWNTs is reasonable. The ab initio calculations present a unique insight onto molecular level interaction of SWNTs; which in essence confirm a more favorable interaction, i.e., higher aggregation propensity (or lower stability), between SG76 tubes compared to SG65. The role of higher diameter in SWNT interaction is also identified as the key mechanism for higher aggregation tendencies of SG76.

The comprehensive characterization and molecular modeling performed in this article has helped to decipher the mechanism of aggregation. The chiral distribution characterization has helped to demonstrate the true chiral enrichments in SG65 and SG76 samples. The electrokinetic measurements along with XPS and Raman spectroscopy demonstrate that the two samples were carefully functionalized with near-equal length and small variation in their electrostatic contribution to aggregation. The molecular modeling further illustrates the higher interaction between larger diameter SG76 tubes compared to those in SG65. These physicochemical characterization and modeling results thus have helped to identify “chirality difference” of semiconducting SG65 and SG76 tubes to be the discerned etiology for the observed aggregation behavior.

Role of SRHA vs Chirality in Aggregation.

Figure 7 shows a decrease in aggregation rate—as calculated from the aggregation profiles (Figure S9)—in presence of 2.5 mg TOC/L SRHA for both mono- and divalent electrolytes at 10 mM ionic strength. The stability enhancement by SRHA under monovalent electrolyte condition is insignificant for both SG65 and SG76. However, mixed electrolyte condition shows substantial increase in stability or decrease in aggregation rate, with SRHA addition; i.e., 70% (from 0.10 ± 0.001 to 0.02 ± 0.006 nm/s) and 25% (from 0.19 ± 0.016 to 0.14 ± 0.027 nm/s) decrease in the rate of aggregation for SG65 and SG76, respectively.

Electrolyte conditions as well as chirality played a significant role in stability enhancement with SRHA. The mechanism can be described through the surface potential of the SWNTs (Figure S10). Though the SRHA addition did not alter the EPM values of SG65 or SG76 in either of the conditions substantially, the overall magnitude of EPM is observed to be lower in presence of divalent electrolyte, as expected (Figure S10). The lower EPM values resulted in higher aggregation rate for both chirality SWNTs (in absence of SRHA); higher for SG76 compared to SG65, following similar trend and aggregation mechanism explained earlier. The notable increase in stability in presence of SRHA is thus attributed to non-DLVO, steric interactions, with little or no electrostatic contribution imparted by the adsorbed humic macromolecules. Such stability enhancement was previously observed for SWNTs[17] as well as for MWNTs[16] and fullerenes.[48,49]

Implication for Fate and Transport in Aquatic Environments.

SWNTs, upon release, will be exposed to mono- and di-valent electrolytes—typical to aquatic environments, e.g., groundwater, surface water, marine environments—and thus necessitate fundamental understanding of aggregation behavior in such conditions. Results from this study suggest that SWNTs are relatively stable with a dominant role of chirality in their stability in a typical aquatic environment. Particularly, semiconducting SWNTs with near-armchair configurations and relatively smaller diameter will likely show higher stability compared to larger diameter tubes. Presence of SRHA is likely to enhance SWNT stability, however, it is also governed by the chirality type of the tubes. The findings also indicate that literature studies on SWNT aggregation with no analysis for its chirality can be unreliable to accurately predict colloidal stability. Moreover, most commercial SWNTs are synthesized and used as unknown mixed chirality systems and therefore can show inconsistent aggregation with respect to their laboratory studied reference behavior. This study involved two chiral specific SWNT samples leaving a large gap in the chirality chart to establish a better and more complete understanding of the role of chirality in SWNT aggregation. The results of this study should be used as the first reference point for chirality influence on semiconducting SWNT aggregation, however, may not be generalized for the entire chirality map. Further systematic studies with chiral specific SWNTs covering a wider region of the chirality chart for both semiconducting and metallic tubes are of great importance.

Supplementary Material

Refer to Web version on PubMed Central for supplementary material.

ACKNOWLEDGMENTS

Funding was provided by the National Science Foundation (CBET 0933484). We are grateful to USC Electron Microscopy Center for its assistance in TEM imaging.

REFERENCES

(1). Forro L; Salvetat J-P; Bonard J-M; Bacsa R; Thomson NH; Garaj S; Thien-Nga L; Gaal R; Kulik A; Ruzicka B; Degiorgi L; Bachtold A; Schönenberger C; Pekker S; Hernadi K In Science and Application of Nanotubes; Tománek D, Enbody RJ, Eds.; Kluwer Academic/Plenum Publishers: New York, 2000.

(2). Saito R; Dresselhaus G; Dresselhaus MS Physical Properties of Carbon Nanotubes; Imperial College Press: London, 1998.

(3). Chen KJ; Nair N; Strano MS; Braatz RD Identification of chirality-dependent adsorption kinetics in single-walled carbon nanotube reaction networks. J. Comput. Theor. Nanosci 2010, 7, 2581–2585.

(4). Baughman RH; Zakhidov AA; de Heer WA Carbon nanotubes - the route toward applications. Science 2002, 297, 787–792. [PubMed: 12161643]

(5). Avouris P Molecular Electronics with Carbon Nanotubes. Acc. Chem. Res 2002, 35, 1026–1034. [PubMed: 12484790]

(6). Lekas D Analysis of Nanotechnology from an Industrial Ecology Perspective Part II: Substance Flow Analysis of Carbon Nanotubes; Woodrow Wilson International Center for Scholars: Washington, DC, 2005.

(7). Shukla PK; Mishra PC Effects of diameter, length, chirality and defects on the scavenging action of single-walled carbon nanotubes for OH radicals: A quantum computational study. Chem. Phys 2010, 369, 101–107.

(8). Thostenson ET; Ren ZF; Chou TW Advances in the science and technology of carbon nanotubes and their composites: A review. Compos. Sci. Technol 2001, 61, 1899–1912.

(9). Zhbanov AI; Pogorelov EG; Chang YC Van der waals interaction between two crossed carbon nanotubes. ACS Nano 2010, 4, 5937–5945. [PubMed: 20863127]

(10). Elimelech M; Gregory J; Jia X; Williams RA Particle Deposition and Aggregation: Measurement, Modelling and Simulation; Elsevier, 1995.

(11). Popescu A; Woods LM; Bondarev IV Chirality dependent carbon nanotube interactions. Phys. Rev. B 2011, 83, 081406(R).

(12). Rajter RF; Podgornik R; Parsegian VA; French RH; Ching WY van der Waals-London dispersion interactions for optically anisotropic cylinders: Metallic and semiconducting single-wall carbon nanotubes. Phys. Rev. B 2007, 76, 045417.

(13). Petosa AR; Jaisi DP; Quevedo IR; Elimelech M; Tufenkji N Aggregation and Deposition of Engineered Nanomaterials in Aquatic Environments: Role of Physicochemical Interactions. Environ. Sci. Technol 2010, 44, 6532–6549. [PubMed: 20687602]

(14). Lin DH; Liu N; Yang K; Zhu LZ; Xu Y; Xing BS The effect of ionic strength and pH on the stability of tannic acid-facilitated carbon nanotube suspensions. Carbon 2009, 47, 2875–2882.

(15). Hyung H; Fortner JD; Hughes JB; Kim JH Natural organic matter stabilizes carbon nanotubes in the aqueous phase. Environ. Sci. Technol 2007, 41, 179–184. [PubMed: 17265945]

(16). Saleh NB; Pfefferle LD; Elimelech M Aggregation Kinetics of Multiwalled Carbon Nanotubes in Aquatic Systems: Measurements and Environmental Implications. Environ. Sci. Technol 2008, 42, 7963–7969. [PubMed: 19031888]

(17). Saleh NB; Pfefferle LD; Elimelech M Influence of Biomacromolecules and Humic Acid on the Aggregation Kinetics of Single-Walled Carbon Nanotubes. Environ. Sci. Technol 2010, 44, 2412–2418. [PubMed: 20184360]

(18). Smith B; Wepasnick K; Schrote KE; Cho HH; Ball WP; Fairbrother DH Influence of Surface Oxides on the Colloidal Stability of Multi-Walled Carbon Nanotubes: A Structure-Property Relationship. Langmuir 2009, 25, 9767–9776. [PubMed: 19583226]

(19). Shieh YT; Liu GL; Wu HH; Lee CC Effects of polarity and pH on the solubility of acid-treated carbon nanotubes in different media. Carbon 2007, 45, 1880–1890.

(20). Sano M; Okamura J; Shinkai S Colloidal nature of single-walled carbon nanotubes in electrolyte solution: The Schulze-Hardy rule. Langmuir 2001, 17, 7172–7173.

(21). Niyogi S; Boukhalfa S; Chikkannanavar SB; McDonald TJ; Heben MJ; Doorn SK Selective aggregation of single-walled carbon nanotubes via salt addition. J. Am. Chem. Soc 2007, 129, 1898–1899. [PubMed: 17253695]

(22). Green AA; Duch MC; Hersam MC Isolation of Single-Walled Carbon Nanotube Enantiomers by Density Differentiation. Nano Res. 2009, 2, 69–77.

(23). Jorio A; Saito R; Hafner JH; Lieber CM; Hunter M; McClure T; Dresselhaus G; Dresselhaus MS Structural (n, m) determination of isolated single-wall carbon nanotubes by resonant Raman scattering. Phys. Rev. Lett 2001, 86, 1118–1121. [PubMed: 11178024]

(24). Itkis ME; Niyogi S; Meng ME; Hamon MA; Hu H; Haddon RC Spectroscopic study of the Fermi level electronic structure of single-walled carbon nanotubes. Nano Lett. 2002, 2, 155–159.

(25). Vardanega D; Picaud F; Girardet C Chiral response of single walled carbon nanotube based sensors to adsorption of amino acids: A theoretical model. J. Chem. Phys 2007, 127.

(26). Li Y; Zhang X; Luo Z; Huang W; Cheng J; Luo Z; Li T; Liu F; Xu G; Ke X; Li L; Geise HJ Purification of CVD synthesized single-wall carbon nanotubes by different acid oxidation treatments. Nanotechnology 2004, 15, 1645–1649.

(27). Liu J; Rinzler AG; Dai H; Hafner JH; Bradley RK; Boul PJ; Lu A; Iverson T; Shelimov K; Huffman CB; Rodriguez-Macias F; Shon Y-S; Lee TR; Colbert DT; Smalley RE Fullerene pipes. Science 1998, 280, 1253–1256. [PubMed: 9596576]

(28). Zaib Q; Khan I; Yoon Y; Flora J; Park Y; Saleh N Systematic ultrasonication study for suspending single-walled carbon nanotubes in water. J. Nanosci. Nanotechnol 2012, 12, 3909–3917. [PubMed: 22852324]

(29). Schierz A; Parks AN; Washburn KM; Chandler GT; Ferguson PL Characterization and Quantitative Analysis of Single-Walled Carbon Nanotubes in the Aquatic Environment Using Near-Infrared Fluorescence Spectroscopy. Environ. Sci. Technol 2012, 46, 12262–12271. [PubMed: 22970987]

(30). Wagner AJ; Wolfe GM; Fairbrother DH Reactivity of vapor-deposited metal atoms with nitrogen-containing polymers and organic surfaces studied by in situ XPS. Appl. Surf. Sci 2003, 219, 317–328.

(31). Haselbach LM; Ma S Potential for carbon adsorption on concrete: surface XPS analyses. Environ. Sci. Technol 2008, 42, 5329–5334. [PubMed: 18754389]

(32). Kohn T; Kane SR; Fairbrother DH; Roberts AL Investigation of the Inhibitory effect of silica on the degradation of 1,1,1-Trichloroethane by granular iron. Environ. Sci. Technol 2003, 37, 5806–5812. [PubMed: 14717199]

(33). Aich N; Flora JRV; Saleh NB Preparation and characterization of stable aqueous higher-order fullerenes. Nano-technology 2012, 23, 055705.

(34). Humphrey W; Dalke A; Schulten K VMD: Visual molecular dynamics. J. Mol. Graphics 1996, 14, 33–38.

(35). Grimme S; Antony J; Ehrlich S; Krieg H A consistent and accurate ab initio parametrization of density functional dispersion correction (DFT-D) for the 94 elements H-Pu. J. Chem. Phys 2010, 132, 154104–154119. [PubMed: 20423165]

(36). Grimme S; Ehrlich S; Goerigk L Effect of the damping function in dispersion corrected density functional theory. J. Comput. Chem 2011, 32, 1456–1465. [PubMed: 21370243]

(37). O'Connell MJ; Bachilo SM; Huffman CB; Moore VC; Strano MS; Haroz EH; Rialon KL; Boul PJ; Noon WH; Kittrell C; Ma J; Hauge RH; Weisman RB; Smalley RE Band Gap Fluorescence from Individual Single-Walled Carbon Nanotubes. Science 2002, 297, 593–596. [PubMed: 12142535]

(38). Saito R; Dresselhaus G; Dresselhaus MS Trigonal warping effect of carbon nanotubes. Phys. Rev. B 2000, 61, 2981–2990.

(39). Weisman RB; Bachilo SM Dependence of Optical Transition Energies on Structure for Single-Walled Carbon Nanotubes in Aqueous Suspension: An Empirical Kataura Plot. Nano Lett. 2003, 3, 1235–1238.

(40). Datsyuk V; Kalyva M; Papagelis K; Parthenios J; Tasis D; Siokou A; Kallitsis I; Galiotis C Chemical oxidation of multiwalled carbon nanotubes. Carbon 2008, 46, 833–840.

(41). Lebron-Colon M; Meador MA; Lukco D; Sola F; Santos-Perez J; McCorkle LS Surface oxidation study of single wall carbon nanotubes. Nanotechnology 2011, 22, 455707. [PubMed: 22020272]

(42). Wepasnick KA; Smith BA; Bitter JL; Fairbrother DH Chemical and structural characterization of carbon nanotube surfaces. Anal. Bioanal. Chem 2010, 396, 1003–1014. [PubMed: 20052581]

(43). Wepasnick KA; Smith BA; Schrote KE; Wilson HK; Diegelmann SR; Fairbrother DH Surface and structural characterization of multi-walled carbon nanotubes following different oxidative treatments. Carbon 2011, 49, 24–36.

(44). Hirsch A Functionalization of single-walled carbon nanotubes. Angew Chem. Int. Ed 2002, 41, 1853–1859.

(45). Sun Y; Fu K; Lin Y; Huang W Functionalized carbon nanotubes: Properties and applications. Acc. Chem. Res 2002, 35, 1096–1104. [PubMed: 12484798]

(46). Hu H; Yu A; Kim E; Zhao B; Itkis ME; Bekyarova E; Haddon RC Influence of the Zeta Potential on the Dispersability and Purification of Single-Walled Carbon Nanotubes. J. Phys. Chem. B 2005, 109, 11520–11524. [PubMed: 16852411]

(47). Smith B; Wepasnick K; Schrote KE; Bertele AH; Ball WP; O'Melia C; Fairbrother DH Colloidal Properties of Aqueous Suspensions of Acid-Treated, Multi-Walled Carbon Nanotubes. Environ. Sci. Technol 2009, 43, 819–825. [PubMed: 19245021]

(48). Chen KL; Elimelech M Aggregation and Deposition Kinetics of Fullerene (C60) Nanoparticles. Langmuir 2006, 22, 10994–11001. [PubMed: 17154576]

(49). Chen KL; Elimelech M Influence of humic acid on the aggregation kinetics of fullerene (C60) nanoparticles in monovalent and divalent electrolyte solutions. J. Colloid Interface Sci. 2007, 309, 126–134. [PubMed: 17331529]

(50). Tucknott R; Yaliraki SN Aggregation properties of carbon nanotubes at interfaces. Chem. Phys 2002, 281, 455–463.

(51). Rajter RF; French RH; Ching WY; Carter WC; Chiang YM Calculating van der Waals-London dispersion spectra and Hamaker coefficients of carbon nanotubes in water from ab initio optical properties. J. Appl. Phys 2007, 101, 054303.

(52). Yi P; Chen KL Influence of Surface Oxidation on the Aggregation and Deposition Kinetics of Multiwalled Carbon Nano-tubes in Monovalent and Divalent Electrolytes. Langmuir 2011, 27, 3588–3599. [PubMed: 21355574]

(53). Autho Department of Materials Science and Engineering, MIT: Cambridge, MA, 2009; Vol. PhD, p 224.

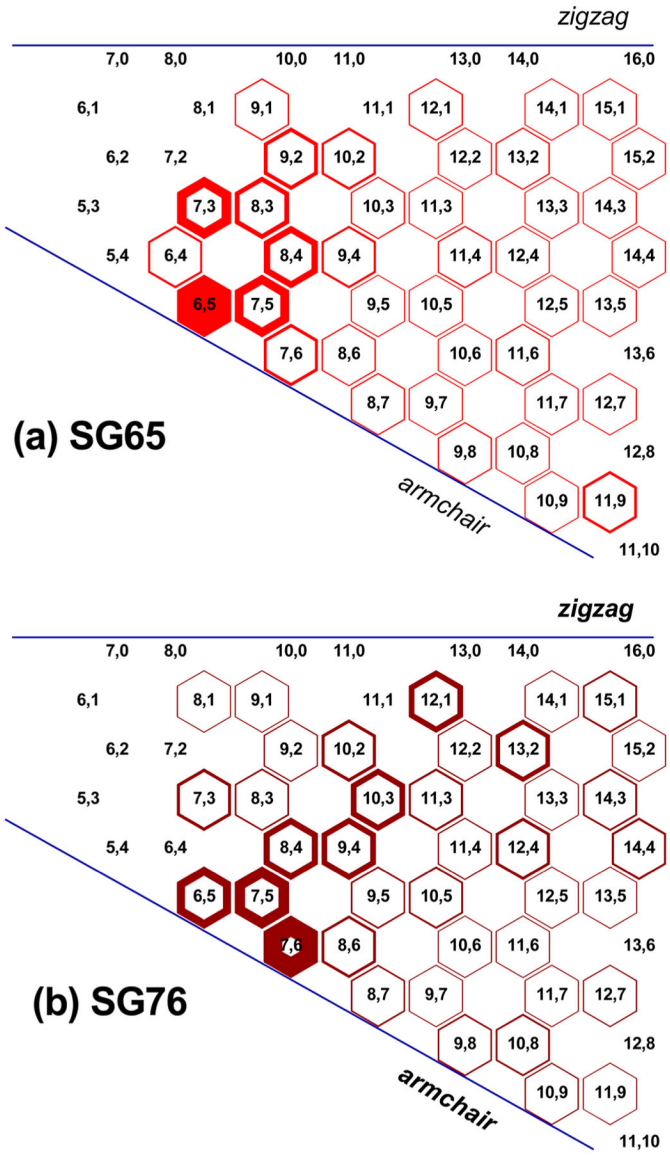

Figure 1.
Chirality charts of (a) SG65 and (b) SG76 SWNTs samples showing chirality distribution.

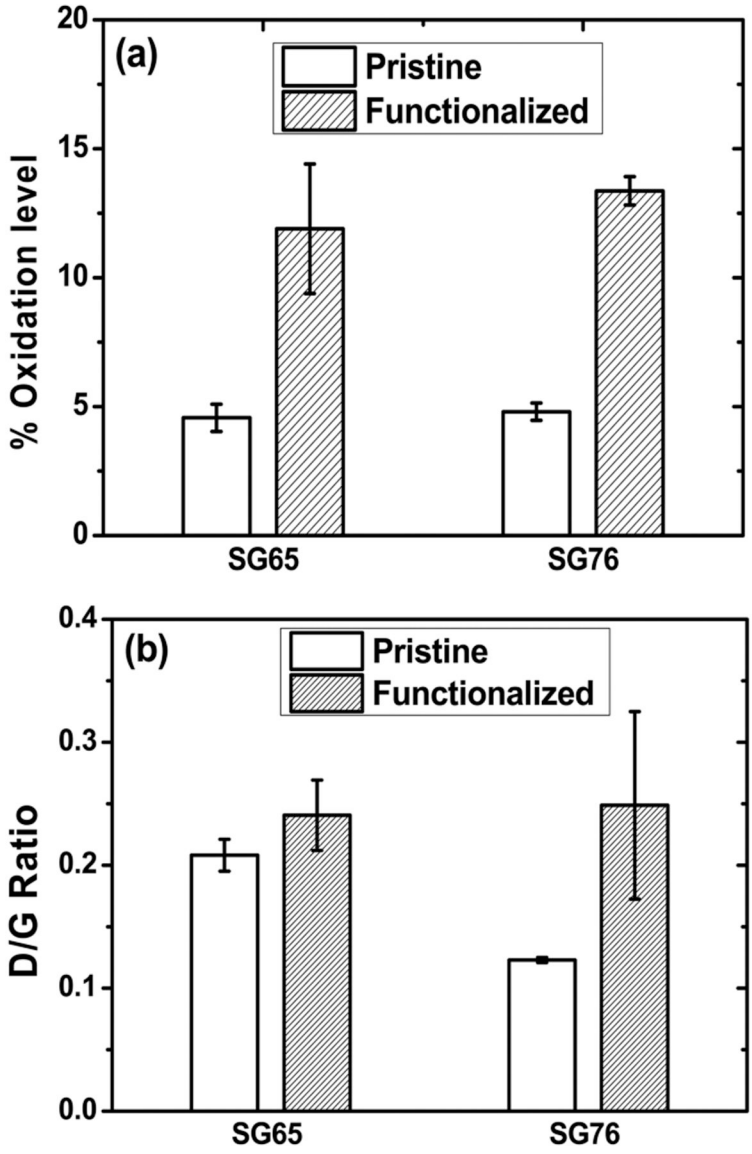

Figure 2.

(a) Average oxidation level of pristine and functionalized SWNTs measured by X-ray photoelectron spectroscopy (XPS). (b) State of defect presented by D/G ratios from Raman spectroscopy. Error bars represent one standard deviation.

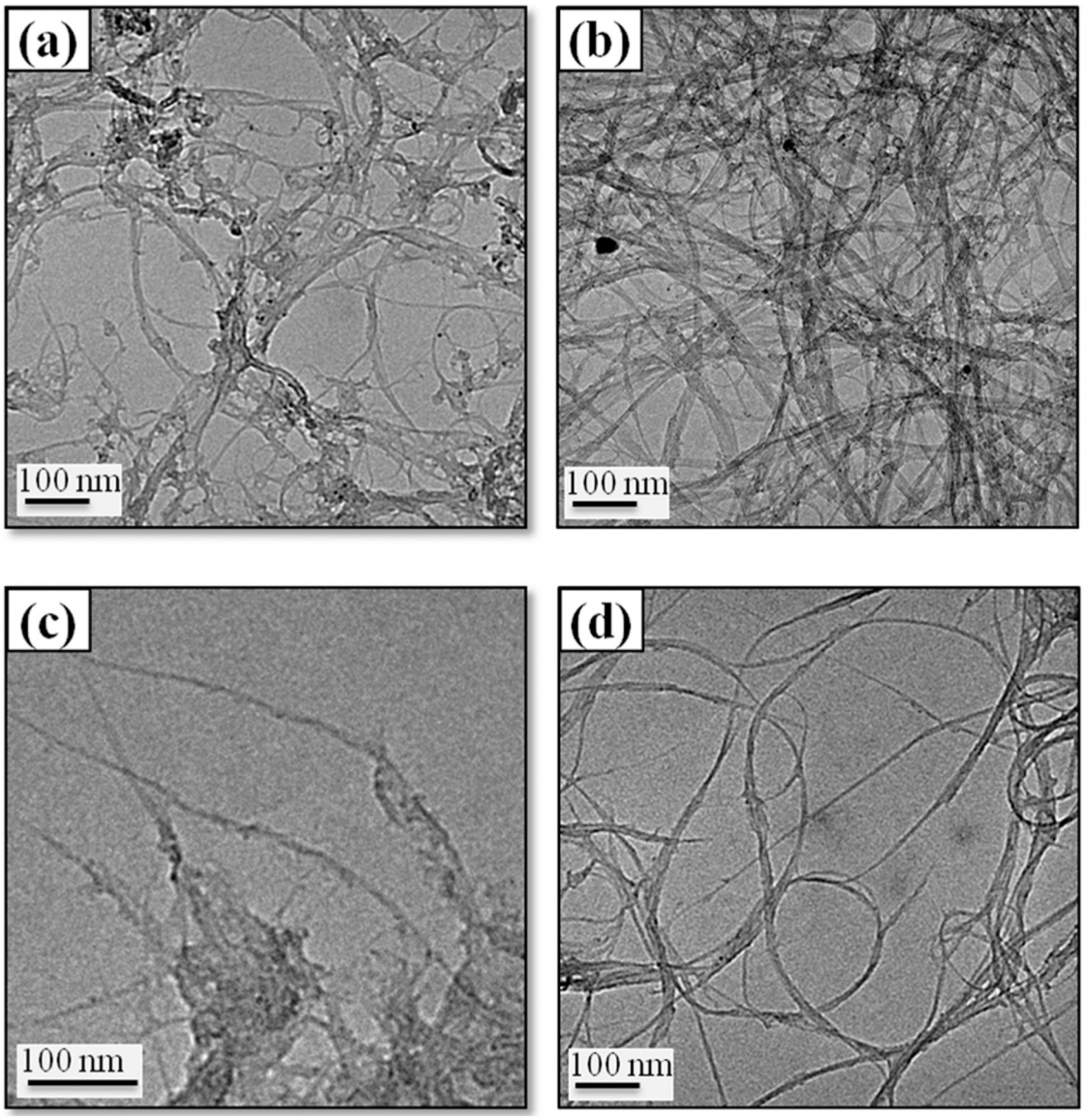

Figure 3.

Representative TEM micrographs of (a−b) pristine and (c−d) functionalized SWNTs. Images on the left are of SG65 and on the right are of SG76 samples.

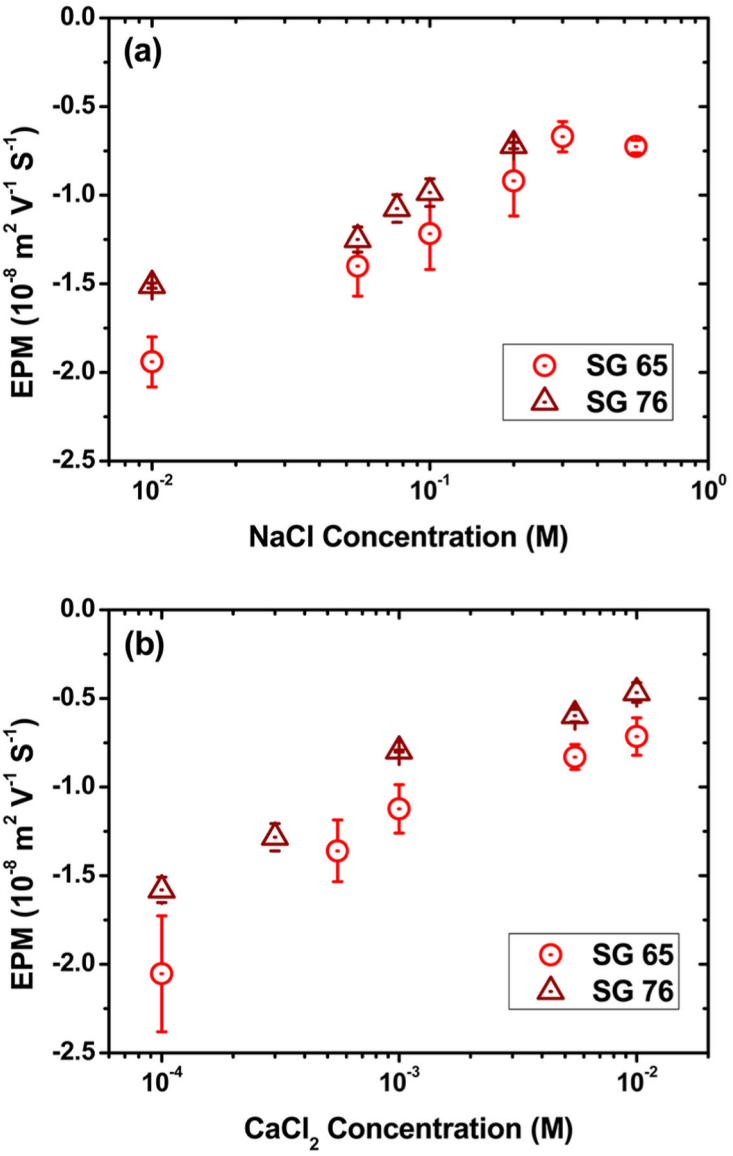

Figure 4.

Electrophoretic mobility (EPM) of functionalized SWNTs as a function of (a) monovalent and (b) divalent salts (NaCl and $CaCl_2$). Measurements were carried out at pH ~6.5 and temperature 20 °C.

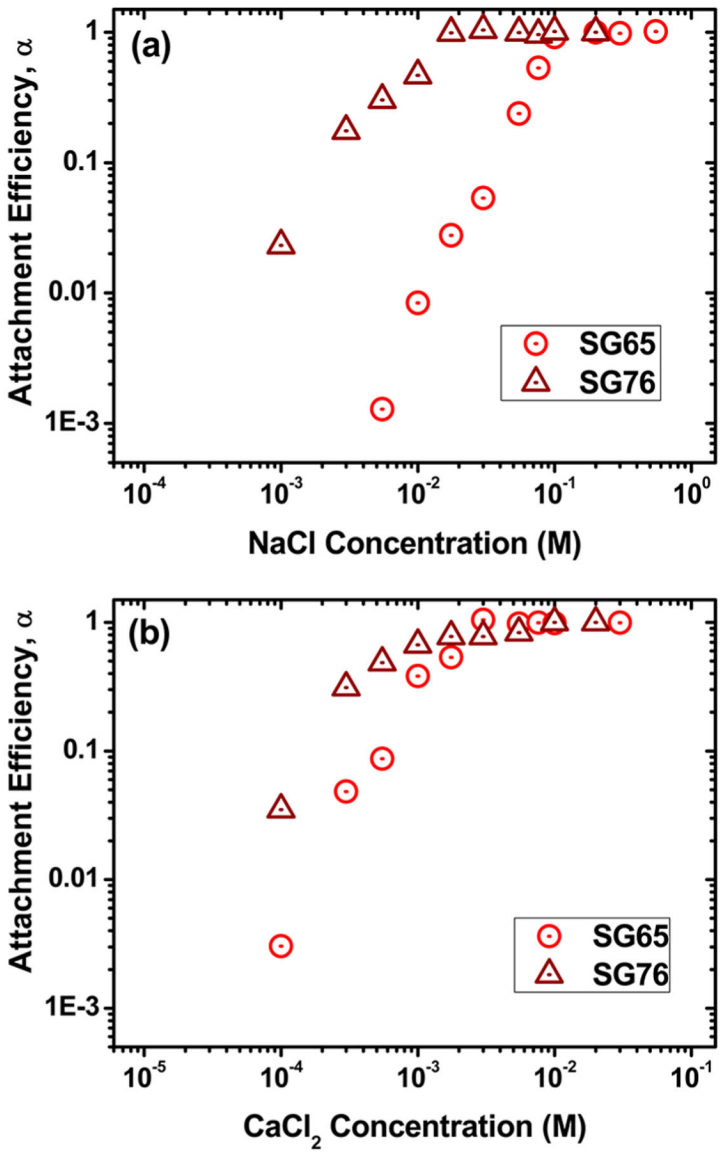

Figure 5.

Attachment efficiencies of functionalized SWNTs as a function of (a) NaCl and (b) $CaCl_2$ salt concentration. Measurements were carried out at pH ~6.5 and temperature 20 °C.

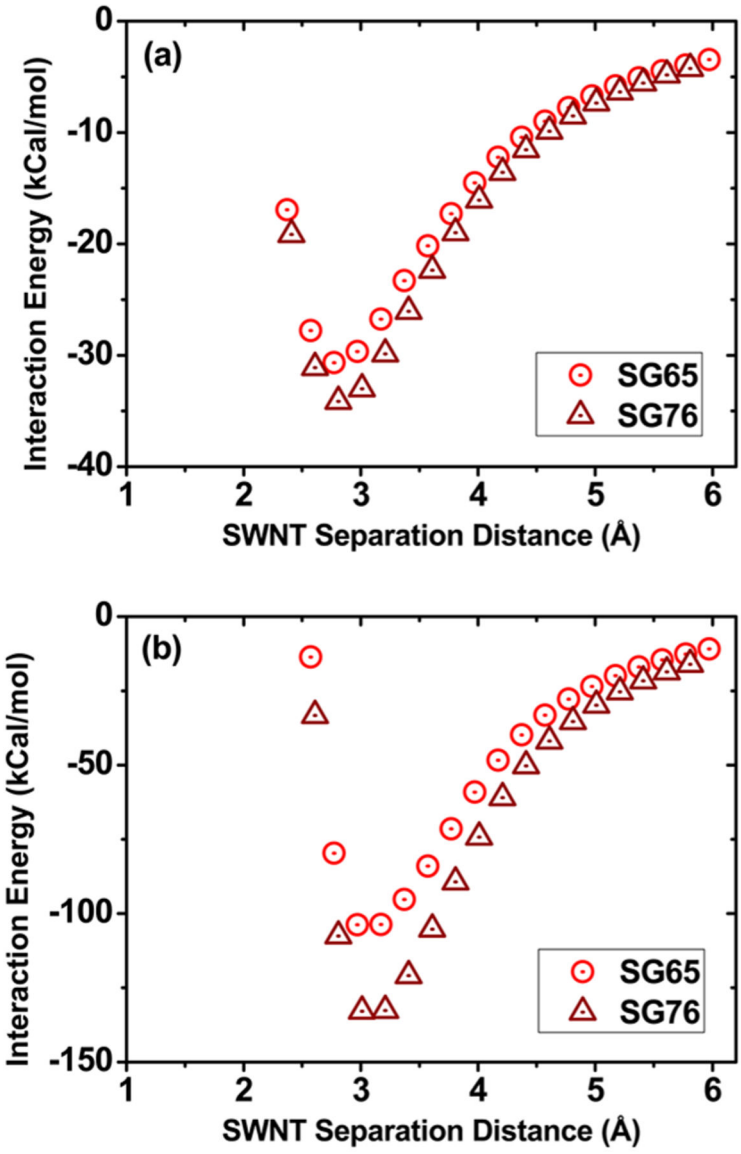

Figure 6.

Interaction energy of SG65 and SG76 SWNTs calculated using dispersion corrected density functional theory (a) perpendicular and (b) parallel configuration.

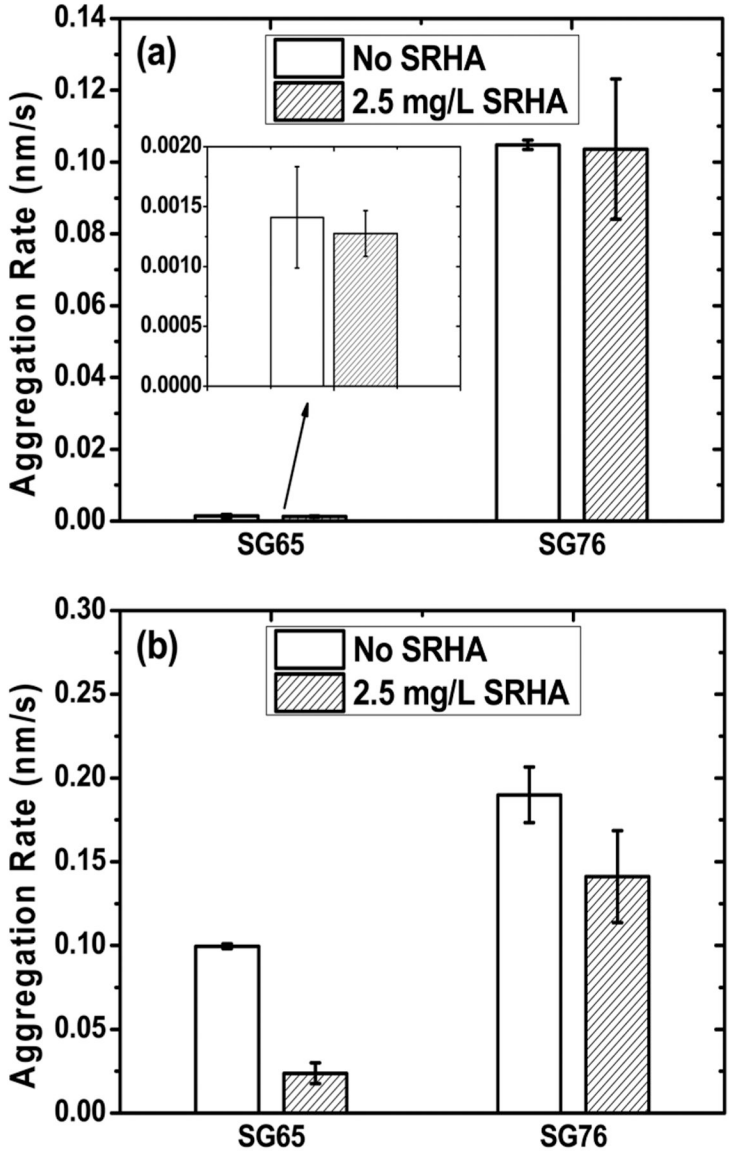

Figure 7.

Initial aggregation rates of SWNTs with (a) 10 mM NaCl and (b) 7 mM NaCl + 1 mM $CaCl_2$ in presence of 2.5 mg TOC/L SRHA. The inset in (a) is a zoomed in plot to represent the rate differences with clarity.